Application of the small-angle approximation to ocean water types

Nancy L. Swanson, Barton D. Billard, Victor M. Gehman, and Theresa L. Gennaro

The small-angle approximation to the radiative transport equation is applied to particle suspensions that emulate ocean water. A particle size distribution is constructed from polystyrene and glass spheres with the best available data for particle size distributions in the ocean. A volume scattering function is calculated from the Mie theory for the particles in water and in oil. The refractive-index ratios of particles in water and particles in oil are 1.19 and 1.01, respectively. The ratio 1.19 is comparable to minerals and nonliving diatoms in ocean water, and the ratio 1.01 is comparable to the lower limit for microbes in water. The point-spread functions are measured as a function of optical thickness for both water and oil mixtures and compared with the point-spread functions generated from the small-angle approximation. Our results show that, under conditions that emulate ocean water, the small-angle approximation is valid only for small optical thicknesses. Specifically, the approximation is valid only for optical thicknesses less than 3.

OCIS codes: 010.4450, 110.4100, 290.7050, 290.4210, 290.5820, 290.4020.

1. Introduction

A previous investigation[1] explored limits of the small-angle approximation (SAA) to the radiative transport equation as a function of particle size and concentration for a particle-to-medium refractive-index ratio of 1.196. The measurements were made for nearly monodisperse (coefficient of variation less than 10%) particle size distributions. In this paper we report results obtained with a distribution of particle sizes chosen to approximate scattering properties measured for ocean water and at refractive-index ratios comparable to values near the upper and lower limits for constituents of ocean water.

The SAA, first formulated by Wells,[2] is widely applied to imaging in optically dense media such as water and fog. This approximation leads to a functional form for the point-spread function (PSF) that can be calculated with a volume scattering function (VSF), also called the scattering phase function, as input. Wells suggested an algebraic form for the VSF, which has been widely used because the PSF solution can then be obtained analytically.[3–5] The resulting PSF is used to predict the amount of blur in an image based on water quality.

Images taken from field and tank tests have shown that this formulation predicts too much blur in the images.[6] Figure 1 is an example of some of the tank test data. The optical thickness was 3.1, the range 6.1 m, and the attenuation coefficient 0.5 m^{-1}. The particles were polystyrene spheres with diameters ranging from 1 to 8 μm. Figure 1(a) is the actual image taken of a reflection panel at the given depth. Figure 1(b) is the image generated from the measured PSF convolved with an image of the reflectance panel taken in air. Figure 1(c) is the image generated from the PSF calculated from the SAA with the Wells algebraic VSF as input, convolved with the image in air. Similar results were obtained from data taken during a field test in San Diego Harbor with an underwater imaging system. The researchers could not determine whether the SAA theory was inadequate or whether the discrepancy was the result of using the Wells VSF.

The Wells VSF has been used to validate the SAA for ocean water data.[3] Subsequently a modified algebraic form that more closely fits the data has been used to model lidar systems.[7] Our research is an effort to determine how robust the SAA is when the VSF is known exactly and the PSF is numerically calculated from the SAA.

N. L. Swanson is with the Society of Photo-Optical Instrumentation Engineers, P.O. Box 10, Bellingham, Washington 98227. B. D. Billard (billardbd@nswc.navy.mil) and T. L. Gennaro are with the Dahlgren Division, Naval Surface Warfare Center, 17320 Dahlgren Road, Dahlgren, Virginia 22448-5100. V. M. Gehman is with the Department of Physics, Virginia Polytechnic Institute, Blacksburg, Virginia 24060.

Received 26 October 2000; revised manuscript received 30 March 2001.

0003-6935/01/213608-06$15.00/0

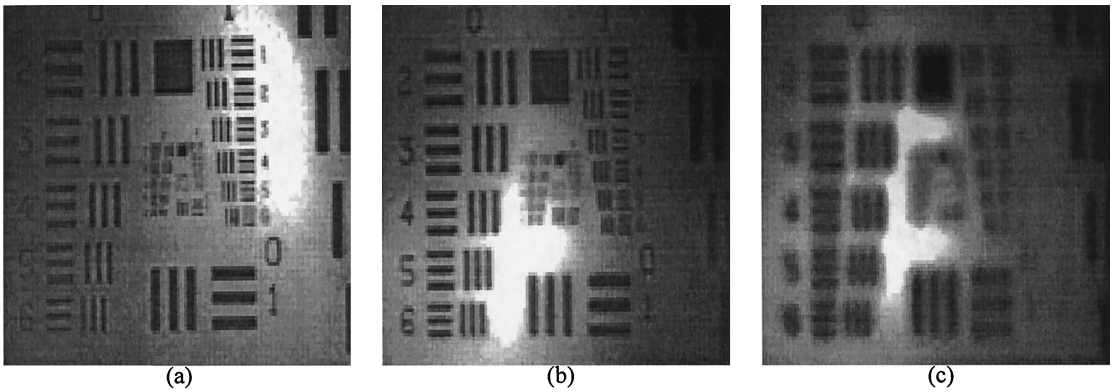

(a) (b) (c)

Fig. 1. Images of standard bar chart panels. (a) The image taken during the tank test with $\tau = 3.05$, a range of 6.1 m, and an attenuation of 0.5 m^{-1}. The medium was water with 1–8-μm polystyrene spheres added. The refractive-index ratio was 1.19. (b) The image generated from an image of the bar chart panel in air convolved with the measured PSF at $\tau = 3.05$. (c) The image generated from an image taken in air convolved with a PSF generated from the SAA with Wells's algebraic VSF as input. Figure reprinted by permission, courtesy of Anne Davenport, Naval Surface Warfare Center, Coastal Systems Station, Panama City, Florida.

2. Background

Application of the SAA to the radiative transport equation results in a linear integrodifferential equation describing the lateral spread of a beam as it propagates through a medium. The equation can then be solved by integral transform techniques.[8] The result is a closed-form expression for the modulation transfer function (MTF) $F(\psi, r)$, where ψ is the spatial frequency in cycles per radian. The PSF $f(\theta, r)$, which describes the power distribution at a range r per unit solid angle at an angle θ off axis divided by the power transmitted, can be obtained by the Hankel transform pairs,

$$f(\theta, r) = 2\pi \int_0^{\infty} J_0(2\pi\theta\psi) F(\psi, r)\psi d\psi,$$

$$F(\psi, r) = 2\pi \int_0^{\theta_{max}} J_0(2\pi\theta\psi) f(\theta, r)\theta d\theta, \qquad (1)$$

where J_0 is the zeroth-order Bessel function and θ_{max} is the maximum allowable angle conforming to the SAA. Wells suggested using $\theta_{max} = 10°$. In practice, θ_{max} would be the half-angle of the field of view of the detector. We obtained the Hankel transform from the reduction of the two-dimensional Fourier transform by invoking symmetry in the ϕ direction. Scattering in ocean water is generally independent of ϕ, even for polarized beams, as long as the angle is small.

Similarly, the VSF and its Hankel transform are given by

$$\sigma(\theta) = 2\pi \int_0^{\infty} J_0(2\pi\theta\psi)\Sigma(\psi)\psi d\psi,$$

$$\Sigma(\psi) = 2\pi \int_0^{\theta_{max}} J_0(2\pi\theta\psi)\sigma(\theta)\theta d\theta. \qquad (2)$$

The VSF can be considered a probability distribution function describing the angular distribution of the scattered light in the single-scattering limit. As such, its normalization is

$$\iint_{4\pi} \sigma(\theta) d\Omega = 1. \qquad (3)$$

According to the Wells formulation, the functional form of the MTF is

$$F(\psi, r) = \exp[-\xi r + s_f r\Sigma(\psi)], \qquad (4)$$

where r is the optical path length in the medium and $\xi = \alpha + s$ is the total attenuation coefficient, with α being the absorption coefficient and s the scattering coefficient.[5] The scattering coefficient in the forward direction is $s_f = s\eta$ with

$$\eta = 2\pi \int_0^{\theta_{max}} \sigma(\theta)\sin(\theta) d\theta. \qquad (5)$$

Because of the configuration of our experimental setup, Eq. (4) represents the collimated spread function of Wells.[5] The dimensionless quantity ξr is the optical thickness τ. In our experiments, we used suspensions containing both polystyrene and glass spheres. For these particles $\alpha = 0$, so Eq. (4) reduces to

$$F(\psi, r) = \exp\{-\tau[1 - \eta\Sigma(\psi)]\}. \qquad (6)$$

We measured PSFs for both particle suspensions at several optical thicknesses. We obtained the VSF from both Mie theory and by measurement, normalizing using Eq. (3). We integrated Eqs. (1) and (2) numerically using Eq. (6) to obtain the PSF for each τ. We then compared the measured PSFs with those predicted by the SAA theory.

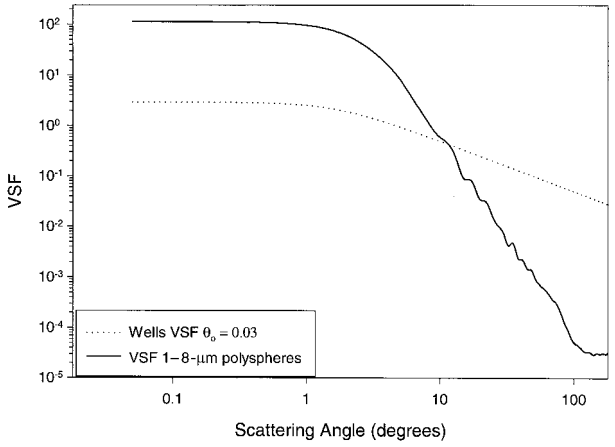

Fig. 2. Comparison of Wells's algebraic VSF with the VSF calculated from Mie theory for 1–8-μm spheres.

3. Experiment

A. Particle Size Distribution

The structure of the VSF is strongly dependent on the refractive-index ratio m (particle to medium) and particle size. If the particles are large compared with the wavelength and optically soft ($m \cong 1$), the scattering will be due mainly to diffraction and refraction and the VSF will be highly peaked in the forward direction. The algebraic function suggested by Wells[5] is given by

$$\sigma(\theta) = \frac{\theta_0}{2\pi(\theta_0{}^2 + \theta^2)^{3/2}}, \tag{7}$$

where θ_0 is an adjustable parameter, typically the average scattering angle. This function is plotted in Fig. 2 versus that generated from Mie theory for the 1–8-μm spheres from the tank test, when we assume an equal number of particles for each size. A comparison of the two curves shows that the Wells VSF represents scattering at larger angles than for the spheres, which would result in more blur.

We constructed a particle size distribution to emulate VSF data taken in ocean water. The distribution comprised polystyrene and glass spheres with a refractive index of 1.58. The refractive-index ratio for the particles is 1.19 in water and 1.01 in oil. We chose the sizes and amounts to match the VSF measured by Petzold[9] at the Tongue of the Ocean (TOTO), Bahamas. The polystyrene spheres comprised ten different samples with mean diameters ranging from 0.2 to 10 μm. The individual polystyrene samples had Gaussian size distributions with coefficients of variation ranging from 2.6% to 10.7%. The glass spheres also had a Gaussian distribution with a mean diameter of 26 μm and a 31.4% coefficient of variation. We chose combinations of various sizes of polystyrene and the glass spheres that gave an overall size distribution consistent with Petzold's VSF data. First, we computed a predicted VSF as a weighted sum of contributions from each individual size distribution. The initial weights used were selected to generate an overall distribution approximating a hyperbolic, or power-law, cumulative distribution, following the approach of Brown and Gordon[10] and Kullenberg.[11] Then we adjusted the weights to generate a VSF close to the measured data of Petzold. Table 1 lists the weights (percentage by number) used for each particle size. The large percentage of the smallest particle size was necessary to increase the VSF at large angles to match the data. We calculated the VSF for the spheres from Mie theory using the known size distribution. The resulting VSFs are compared with Petzold's data and with the modified Wells function in Fig. 3. The modified Wells function is given by[7]

$$\sigma(\theta) = \frac{1}{\theta^{3/2}(\theta_0{}^2 + \theta^2)^{1/2}}. \tag{8}$$

The modified Wells function is a much better fit to the measured data. The VSF for the spheres in water is also a good fit, except at angles smaller than 0.3 deg. The VSF for the spheres in oil is not as good, but the overall shape is plausible.

Table 1. Particle Sizes and Weights (percentage by number) used to Simulate Ocean Water

Mean Diameter (μm)	Coefficient of Variation (%)	Weights (%)
0.202	2.9	95.0
0.527	5.1	0.527
3.359	3.4	0.252
3.9	3.5	0.065
4.003	3.5	0.394
5.292	4.1	0.246
6.2	10.0	0.380
7.924	10.7	0.846
9.64	7.4	0.640
26.1	31.4	1.42

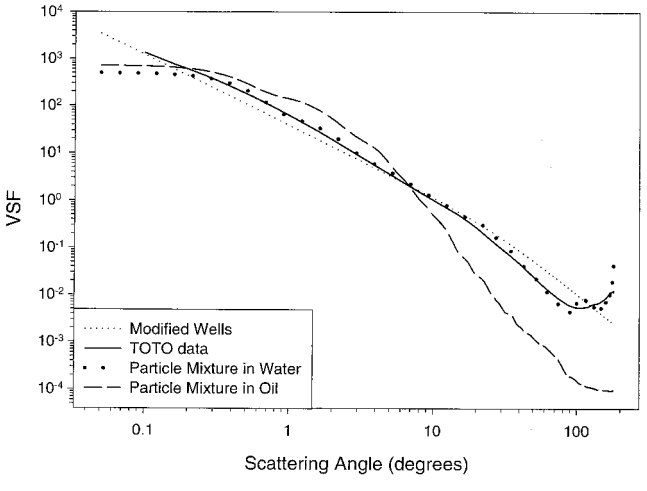

Fig. 3. Comparison of VSF calculated from the particle size distribution with measured TOTO data, along with the modified Wells VSF.

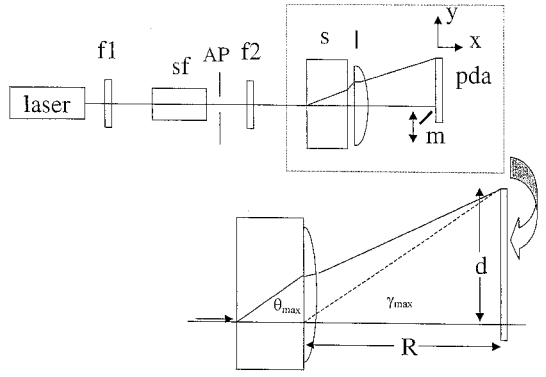

Fig. 4. Experimental setup for measuring the VSF. The components are f1, a fixed neutral-density filter; sf, a spatial filter and collimator; AP, an aperture; f2, removable neutral-density filters; s, the sample cell; l, a lens; pda, a photodiode array detector; m, a small mirror on a translation stage to block and unblock the main beam.

B. Volume Scattering Function

As described in detail in Ref. 1, we adopted the method of Spinrad *et al.*[12] With this technique, taking data at two concentrations and subtracting the results, we minimize excess noise that is due to the lack of beam collimation and stray reflections from the optical components.

In our experiment, we measured the scattered energy with a photodiode array. The received scattered energy was measured along the y direction (see Fig. 4) for the two concentrations. As outlined in Ref. 1, the equation we used to obtain the VSF from the measured data was

$$\sigma(\theta) = \frac{E_2(\theta)/E_2'(0) - E_1(\theta)/E_1'(0)}{(\tau_2 - \tau_1)\,\frac{a}{R^2}\cos^3[\arctan(y/R)]}. \qquad (9)$$

In Eq. (9), $E_2(\theta)/E_2'(0)$ and $E_1(\theta)/E_1'(0)$ are the ratios of the scattered energy at the angle θ to the transmitted energy of the main beam at each concentration (the prime serves to distinguish the transmitted main beam from the scattered energy that would be measured at a zero scattering angle, if the measurement could be made). In the denominator, $\tau_2 - \tau_1$ is the difference in optical thickness measured at the two concentrations found from $\tau_i = -ln[E_i'(0)/E_0'(0)]$, where $E_0'(0)$ is the transmission of the main beam at zero concentration. The remainder of the denominator is the solid angle of scattered radiation received by a detector of area a in the focal plane of a lens of focal length R, where y is the distance along the y axis at the location of the pixel. We converted the y axis along the photodiode from length to scattering angle θ by setting the pixel number of the unscattered peak to zero and using

$$\theta_{\max} = \arcsin\left\{\frac{n_1}{n_2}\sin\left[\arctan\left(\frac{d}{R}\right)\right]\right\} \qquad (10)$$

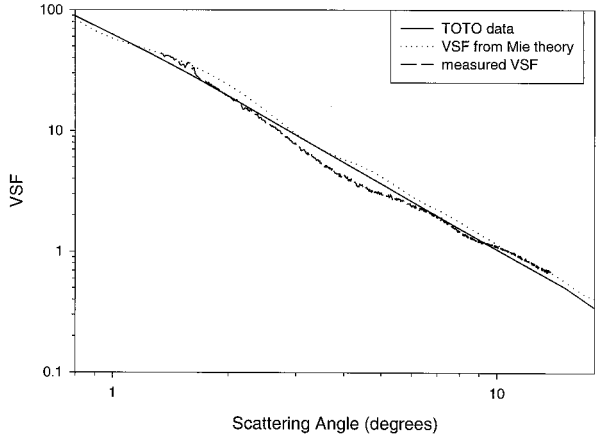

Fig. 5. Measured VSF for particle distribution in water, $m = 1.59$, compared with calculated VSF and TOTO data.

for the maximum pixel number, where $n_1 = 1$ is the refractive index of air and $n_2 = 1.33$ is the refractive index of water. The distance along the photodiode is $d = (t - p)y_{\text{pix}}$, where t is the total number of pixels, p is the pixel number where the unscattered peak is located for any given measurement, and y_{pix} is the size of a single pixel. In our experiment, $t = 1024$, $y_{\text{pix}} = 25\ \mu\text{m}$, and the focal length of the lens $R = 7.6$ cm, which yields $\theta_{\max} \cong 14°$, depending on the location of the unscattered peak.

The size of the sample cell was 5 cm × 2 cm. The laser was a helium–neon laser operating at 633 nm. The photodiode detector was connected to a 16-bit analog-to-digital converter for digitized data collection and storage. To minimize the shot noise in the photodiode detector, the exposure time was maximized so that the peak signal was just below saturation level. We took a dark reading before each data run and performed a background subtraction on each trace to minimize pattern and dark noise. In addition to minimizing noise that is due to the lack of collimation and multiple reflections, when data are taken at two concentrations and the results are sub-

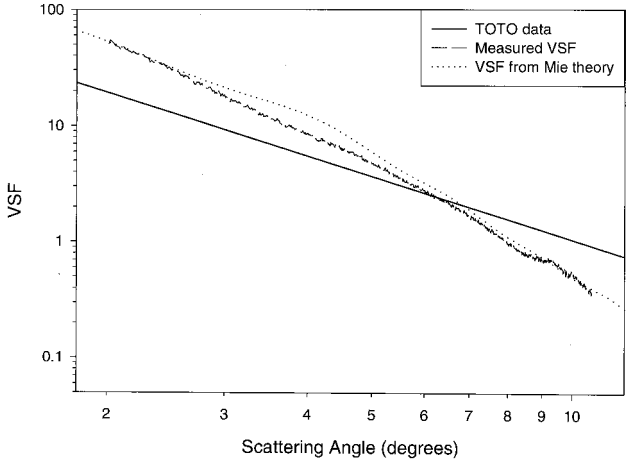

Fig. 6. Measured VSF for particle distribution in oil, $m = 1.01$, compared with calculated VSF and TOTO data.

tracted, as shown in Eq. (9), readout and electronic noise are also reduced.

Figures 5 and 6 show the results for the particle suspension in water and in oil, respectively. Data are not available for $\theta < 2°$ because of the necessity of blocking the main, unscattered beam. Also plotted on the curves are the calculated Mie functions and the TOTO data. Because the measured curves do not exactly match the Mie curves, we used the measured VSF as input to the transform in Eqs. (2) rather than the theoretical curve. The measured portion of the curve was substituted into the Mie curve in the interval $\theta_{min} < \theta < \theta_{max}$, and the entire curve was renormalized according to Eq. (3).

C. Point-Spread Function

The geometry of the experimental setup in Fig. 4 is equivalent to the arrangement for measuring the collimated spread function of Wells.[5] The PSF is defined as the power per unit solid angle Ω, measured off axis at angle θ, per unit power transmitted. Therefore the measured PSF is obtained from

$$f(\theta, L) = \frac{P(\theta, L)}{P_0 \Omega} = \frac{E(\theta, L)}{E_0 \dfrac{a}{R^2} \cos^3[\arctan(y/R)]}. \quad (11)$$

With the proper normalization, the PSF can also be used as a probability distribution function in the same manner as the VSF. In general, the experimental setup in Fig. 4 measures the PSF. In the limit as $\tau \to 0$, except for a normalization factor, the Hankel transform of Eq. (6) returns the VSF and a delta function at $\theta = 0$ representing the transmitted, unscattered light.

We used the same procedure for measuring the PSF as for the VSF, except we continued to add particles between measurements up to $\tau \approx 5$. The approximate values of τ at which measurements were made were 0.5, 1, 1.5, 2, 3, 4, and 5. The VSFs were used as input to Eqs. (2) and (5). Equations (1)–(6) were used to numerically calculate the PSF.

There is some question about the limits in the integral in Eqs. (2). Wells suggested using $\theta_{max} = 10°$ because $\sin\theta \approx \theta$ is valid in the range from 0° to 10°.[5] In practice, the integration interval is typically taken from 0° to 180°, instead of 0°–θ_{max}, because the scattering is assumed to be highly peaked in the forward direction, which would make the contribution to the integral in the interval θ_{max}–180° negligible.[3,5,7] The more accurate results are obtained for the PSF by use of the interval 0°–180°.[1,13] We integrated over the interval and 0°–180°, except when calculating the fraction of scattered light in the forward direction in Eq. (5), where θ_{max} was 14°. Results are presented in Figs. 7 and 8. The solid curves represent the theoretical curves and the dashed curves are the measured data. Both the data and the theory are normalized to unity at an angle of 2 deg. The measured values of τ for each set of curves are shown to the right of the curves. Each set of curves is artificially offset by 2^n so all the sets can be shown on one plot. The percent error between the experimental and theoretical values at an angle of 10.5° is indicated for each set of curves. When we assume that an error of 10% is the maximum tolerance, the SAA is robust only for $\tau < 3$.

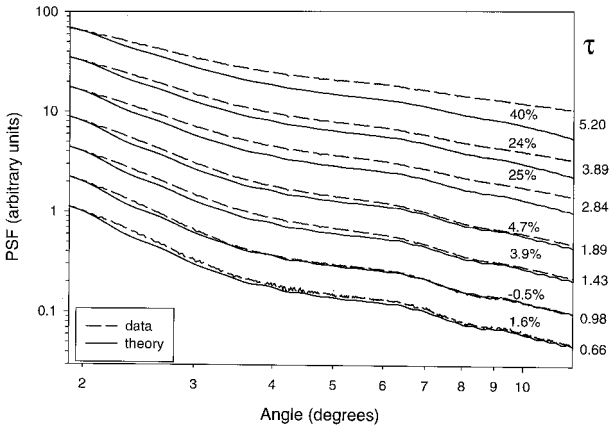

Fig. 7. Measured PSF compared with PSF from the small-angle theory for particles in water. Each set of curves corresponds to a value of τ shown at the right.

Because the theoretical Mie curves did not match the measured VSF curves exactly, some additional error may have been introduced in the transform. On the other hand, normalizing the curves at 2° results in a smaller error than if we had been able to normalize the curves to unity at 0°. Therefore, although the absolute errors may be offset by some systematic errors, the relative errors exhibit clear trends.

The values for the data are greater than the values for the theory at 10.5° for the particles in water, whereas the opposite is true for the particles in oil. The SAA theory underpredicts the blur in an image when the refractive index of the particles differs significantly from that of the medium, as shown for the

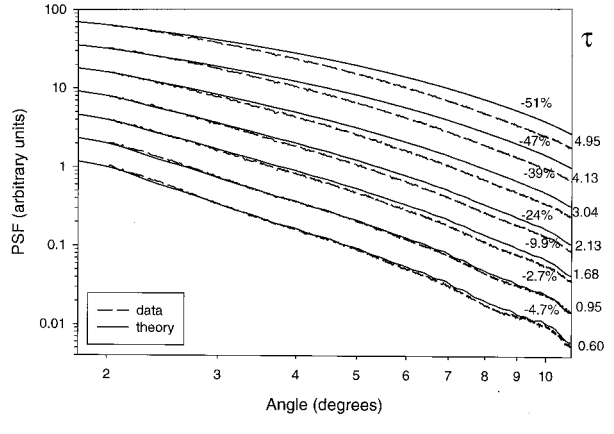

Fig. 8. Measured PSF compared with PSF from the small-angle theory for particles in oil. Each set of curves corresponds to a value of τ shown at the right.

particles in water. Conversely, the theory overpredicts the blur when the refractive index of the particles is close to that of the medium, as shown for the particles in oil. The underprediction and overprediction are better illustrated when we consider the Fourier transform of the PSF, the MTF. The MTF is a measure of the relative contrast in an image of a bar chart placed in such a medium, typically as a function of line pairs per millimeter (in our case, line pairs per radian). If the PSF is wide, the MTF will be narrow, indicating poor contrast (more blur). If the PSF is narrow, the MTF will be wide, indicating good contrast (less blur).

4. Conclusions

We have shown that the SAA theory is accurate only for small optical thicknesses, $\tau < 3$. This is reasonable because $\tau = 3$ corresponds to an average of three scattering events for a photon traversing the medium. Even if the scattering angle were small for individual events, multiple events would lead to larger overall scattering angles. For optically soft particles $m \approx 1$, the theory overpredicts the blur in an image, whereas for particles with $m > 1$, the theory underpredicts the blur. Therefore the excess blur in Fig. 1(c) is due solely to the choice of the VSF used as input to the theory. The SAA theory is sensitive to the structure of the VSF. Even if the exact form of the VSF is known, this theory should be applied with caution for large optical thicknesses. It may be possible that, for a mixture of optically soft particles with minerals and diatoms, the two errors would offset, leading to a more accurate prediction of blur than for either particle type alone.

This research was supported by the U.S. Office of Naval Research. The authors are deeply grateful to Francisco Santiago for many helpful conversations.

References and Notes

1. N. L. Swanson, V. M. Gehman, B. D. Billard, and T. L. Gennaro, "Limits of the small-angle approximation to the radiative transport equation," J. Opt. Soc. Am. A **18,** 385–391 (2001).
2. W. H. Wells, "Loss of resolution in water as a result of multiple small-angle scattering," J. Opt. Soc. Am. **59,** 686–691 (1969).
3. J. W. McLean and K. J. Voss, "Point-spread function in ocean water: comparison between theory and experiment," Appl. Opt. **30,** 2027–2030 (1991).
4. J. W. McLean, D. R. Crawford, and C. L. Hindman, "Limits of small-angle scattering theory," Appl. Opt. **26,** 2053–2054 (1987).
5. W. H. Wells, "Theory of small-angle scattering," in *Optics of the Sea*, AGARD Lect. Ser. **61,** 3.3-1–3.3-19 (1973).
6. In 1994 A. R. Davenport and M. E. Stefanov (Dahlgren Division, Naval Surface Warfare Center, Va.; and Coastal Systems Station, Panama City, Fla.) observed that application of the small-angle approximation, using the Wells phase function as input, did not correspond with their observed data, as shown in Fig. 1.
7. J. W. McLean and J. D. Freeman, "Effects of ocean waves on airborne lidar imaging," Appl. Opt. **35,** 3261–3269 (1996).
8. D. Arnush, "Underwater light beam propagation in the small-angle-scattering approximation," J. Opt. Soc. Am. **62,** 1109–1111 (1972).
9. T. J. Petzold, *Volume Scattering Functions for Selected Ocean Waters* SIO Ref. 72–78 (Visibility Laboratory, Scripps Institution of Oceanography, San Diego, Calif., 1972).
10. O. B. Brown and H. R. Gordon, "Size–refractive index distribution of clear coastal water particulates from light scattering," Appl. Opt. **13,** 2874–2881 (1974).
11. G. Kullenberg, "Observed and computed scattering functions," in *Optical Aspects of Oceanography*, N. G. Jerlov and N. E. Steemann, eds. (Academic, New York, 1974), pp. 25–49.
12. R. W. Spinrad, J. R. V. Zaneveld, and H. Pak, "Volume scattering function of suspended particulate matter at near-forward angles: a comparison of experimental and theoretical values," Appl. Opt. **17,** 1125–1130 (1978).
13. Y. Kuga, A. Ishimaru, H. W. Chang, and L. Tsang, "Comparisons between the small-angle approximation and the numerical solution for radiative transfer theory," Appl. Opt. **25,** 3803–3805 (1986).